Characterization and modeling of chemical reactions taking place during the vitrification of high level waste in cold crucible

Kolani Paraiso, Emilien Sauvage, Sophie Schuller, Virginie Lemaitre, Ekaterina Burov

Characterization and modeling of chemical reactions taking place during the vitrification of high level waste in cold crucible

K. Paraiso[a,*], E. Sauvage[a], S. Schuller[a], V. Lemaitre[a] and E. Burov[b]

[a]CEA, DES, ISEC, DE2D, Univ Montpellier, Marcoule, France
[b]Surface du Verre et Interfaces (UMR 125), CNRS/Saint-Gobain Recherche, 39 quai Lucien Lefranc, Aubervilliers 93300, France

ARTICLE INFO

Keywords:
Nuclear waste
Vitrification
Chemical reactions
Modeling
Phenomenology

ABSTRACT

Several chemical reactions take place during the vitrification of high-level nuclear waste. The integration of these chemical aspects in CFD codes is today one of the key points in the process of improving the prediction capabilities of numerical tools. In this study, based on simultaneous differential thermal analysis-thermogravimetry (DTA–TGA) and run/rerun method, we propose a modeling of the kinetics of chemical reactions taking place when the nuclear glass precursors are subject to constant heating rates. For the mathematical modeling, a weighted sum of n-order reactions is used to describe the overall mechanism. A hybrid approach coupling Kissinger and least squares method is performed to identify the apparent kinetic parameters. Along with the thermal characterization, we also propose a qualitative analysis of the reactions phenomenology through microstructural evolution and evolved gaz analysis based respectively on scanning electron microscope (SEM) and thermogravimetry–mass spectrometry (TGA–MS).

1. Introduction

The calcination-vitrification process has been used in France for over 30 years for the containment of high-level nuclear waste [1–3]. As a first step, calcination process ensures the evaporation and drying of radioactive effluents and the partial decomposition of the salts contained in the solution. The dry residue from the calcination arrives continuously in the vitrification melter (induction heated metal melter and cold crucible induction melter) which is also fed discontinuously with alumino-borosilicate glass frits. The latter provides the chemical elements necessary for the vitreous network formation.

As well in the context of commercial or nuclear glasses, the use of mathematical models for the vitrification process simulation has become widespread in recent years [4–9]. Nevertheless, the modeling of the chemical aspects taking place during the glass synthesis, remains one of the main points of the mathematical models improvement and for optimizing the process control parameters. As recently recalled by Pokorny et *al.* [10], the different approaches used to describe chemical reactions evolution during the glass synthesis, can be classified into two groups: heat-transfer limited model or batch conversion kinetics limited models, according to the mechanism limiting the conversion rate and phenomena that we are trying to model.

In nuclear glass synthesis context, based on simultaneous differential scanning calorimetry-thermogravimetry (DSC–TGA), Chun et *al.* [11] investigated cold-cap reactions in an electrical glass-melting furnace. In this work, the conversion degree of the overall mechanism is then defined based on the reaction net heat flow insulated using Primig and Leitner method [12]. Porkony et *al.* [13] and Suneel et *al.* [14] propose a modeling of cold cap gas-evolving reactions based on thermogravimetric measurements. From mathematical point of view, the n^{th} order kinectic law is used in these works to describe the overall reaction mechanism. The apparent kinetic parameters are estimated using Kissinger method [15] combined with least squares method.

In this paper, we investigate the chemical reactions taking place during the vitrification of high level nuclear waste arasing from the reprocessing of Uranium oxide (UOx) spent fuel. Through simultaneous differential thermal analysis-thermogravimetry (DTA –TGA) and the run/rerun method [11], we propose a characterization of the reaction mechanism between nuclear glass precursors (alumino-borosilicate glass frit and the calcine) when the latter are subjected to a heating process up to 1200 °C at different constant heating rates. By using thermogravimetry analysis coupled with mass spectrometry (TGA-MS) and Scanning Electron Microscope (SEM), an identification approach of the reactions highlighted by DTA-TGA measurements is perfomed based on the analysis of the microstructural evolution and the gases produced by the reactions. In the perspective of integrating these chemical aspects in CFD simulations of vitrification process in cold crucible, we also propose a mathematical modeling of the main reactions kinetics.

2. Experiments

2.1. Sample description

The sample used in this study is composed of a mixture of crushed alumino-borosilicate glass frits (76%) and calcine (24%). The term calcine is used to denote the dry residue from the calcination of simulated high level liquid waste from UOx spent fuel reprocessing. The chemical composition and the mass ratio are similar to that mentioned in the work of Pinet et *al.* [16] and are representative of R7T7 glass produced on an industrial scale [17, 18]. It is important to underline that at the

exit of the calciner, some elements are still present in form of nitrate, oxynitrate, hydroxide or acid and will finish their transformation into oxide in the glass bath. A mixture of precursors is used in this study in order to be as representative as possible of the chemical systems involved in the vitrification process on industrial scale, despite the fact that this will highlight some thermal events (dehydration, melting of some elements at low temperature) which under nominal vitrification conditions do not take place. The evolved gas analysis, as discussed in subsection 4.3, made it possible to discern these effects.

2.2. DTA-TGA measurements

With the aim of studying qualitatively all reactions, whether associated with mass loss or not, simultaneous differential thermal analysis-thermogravimetry (DTA–TGA) is used to describe the overall reaction mechanism. Non-isothermal measurements at different heating rates (5, 10, 20, 30, 40 °C/min) are performed using TAG 2400 (KEP Technologies), equipped with an alumina crucible. For each experiment, approximately 50 mg of sample was loaded into crucible. The measurements were carried out under inert atmosphere in order to identify only the reactions between the precursors. Argon was used as a purge gas. To isolate the net heat flow associated with reactions from that linked with the instrinsec heat capacity of the sample, the run/rerun method [11] is used. This procedure consists in subjecting the sample to two consecutive temperature ramps up to 1200 °C separated by a cooling phase and assume that all the reactions take place during the first run.

2.3. SEM and MS-TGA analyses

In order to identify the microstructural evolution associated with the thermal events revealed by DTA-TGA measurements, the mixture is heated at 10 °C/min in a hot muffle furnace. To ensure the best thermal homogeneity possible of the sample, small volume crucibles identical to those used for DTA-TGA measurements are used. The heat treatment is stopped at different temperatures and samples were analysed by scanning electron microscope after cooling at room temperature. The analyses were performed using a VEGA3 TESCAN device equipped with BSE detector running at 15 kV. The evolved gas analysis were performed using a simultaneous TGA-MS system composed of a thermogravimetric measurement device (SETSYS-TGA) coupled to mass spectroscopy (MS-Supersonic). The sample is placed in an alumina crucible heated from room temperature to 1200 °C at 30 °C/min. The evolved gas are collected in the TGA chamber, near the crucible. Through a two-stage vacuum depressurization system, the gases are almost instantly transmitted to the ionization source of the mass spectrometer. This technique allows to reach a high speed, thus limiting any condensation or recombination.

3. Mathematical modeling

In a large number of pratical case, the reaction rate determined by thermal analyses can be described as function of temperature and conversion degree [19]:

$$\frac{d\alpha_i}{dt} = K(T)f(\alpha_i) \tag{1}$$

Where α_i [-] is the conversion degree, $K(T)$ [s^{-1}] the reaction rate constant in depending on temperature, T [K] the temperature and f the reaction kinetic law. n^{th} order law can be used to describe most of solid-state reactions [11, 13, 14, 20]. Furthermore, if we assume that the dependence of the reaction rate constant on temperature follows Arrhenius' law [21], the reaction rate of chemical reactions taking place during the vitrification of high level nuclear waste can be described by:

$$\frac{d\alpha_i}{dt} = A_i exp\left(-\frac{E_i}{RT}\right)\left(1-\alpha_i\right)^{n_i} \tag{2}$$

With n_i [-] the reaction order, A_i [s^{-1}] the pre-exponential factor, E_i [J mol^{-1}] the activation energy, R [J mol^{-1} K^{-1}] the ideal gases constant and t [s] the time. Under non-isothermal conditions at constant heating rate, the equation 2 can be expressed as :

$$\frac{d\alpha_i}{dT} = \frac{A_i}{\beta} exp\left(-\frac{E_i}{RT}\right)(1-\alpha_i)^{n_i} \tag{3}$$

β [K s^{-1}] represents the heating rate. To estimate the value of the conversion degree, instead of using the approximations of temperature integral proposed in the literature [22–25], we opt here for a finite difference discretization of equation 3. This allows a finer approximation of the temperature integral for a sufficiently small time step. Assuming that the reactions are independent of each other, the reaction rate of the overall mechanism is therefore expressed as:

$$\frac{d\alpha}{dt} = \sum_{i=1}^{N} \alpha_i = \sum_{i=1}^{N} w_i A_i (1-\alpha_i)^{n_i} exp\left(-\frac{E_i}{RT}\right) \tag{4}$$

$$\sum_{i=1}^{N} w_i = 1 \tag{5}$$

α [-] represents the overall progress, w_i [-] the weight factor of each elementary reaction, N the number of reactions. The latter corresponds to the number of local extremum (peaks and shoulders). Kissinger method is commonly used to determine the activation energy (E_i) of each reaction. This is performed by using:

$$\frac{E_i}{R} = -\frac{d\left(ln\left(\beta/T_{pi}^2\right)\right)}{d\left(1/T_{pi}^2\right)} \tag{6}$$

Where T_{pi} [K] is the temperature associated with the characteristic peak of the reaction i. The other apparent kinetic parameters (A_i, n_i, w_i) can be determined by least squares method.

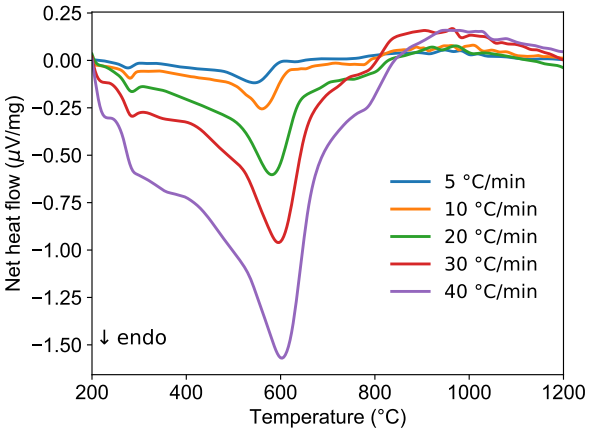

Figure 1: Net heat flow versus temperature for different heating rates. The mention "endo" indicates the direction of endothermic events heat flow.

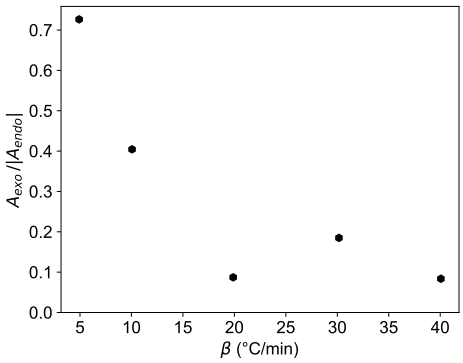

Figure 2: Evolution of the ratio $A_{exo}/|A_{endo}|$ with the heating rate. A_{exo} denotes the area under the exothermic part and $|A_{endo}|$ the absolute value of the area under the endothermic part.

4. Results and discussion

4.1. TDA/TGA results

Figure 1 shows the net heat flux associated with reactions taking place over the temperature range from 200 °C to 1200 °C for the five heating rates. Events occurring before the lower limit of this range are voluntarily ignored in order to avoid the reactions associated with the evaporation of humidity accumulated in the sample. The heat flow profiles reveal a succession of several peaks and shoulders, evidence of a complex mechanism. The latter is composed of endothermic events with a major peak around 600 °C and an exothermic dome after 800 °C. The endothermic events are due of two types of reactions:

- Those which, as discussed in section 4.3, are associated with a mass loss in particular the thermal decomposition of the nitrates still present in calcine and the remaining part of dehydration mechanism.
- Those which do not cause a mass loss, among others the softening of glass frit, the melting of sodium nitrate still present in calcine which in its pure state has a decomposition temperature of 320 °C [26].

Exothermic events could be associated with the formation of crystalline phases [26, 27]. Figure 2 illustrates the evolution of the ratio $A_{exo}/|A_{endo}|$ with the heating rate. A_{exo} denotes the area under the exothermic part and $|A_{endo}|$ the absolute value of the area under the endothermic part. As we can see, the area under the exothermic part of the reaction mechanism seems to decrease when the heating rate increases. This expects that inside the cold crucible where the heating rates are relatively high due to the presence of mechanical stirring and bubbling, the endothermic phase will be predominant from a thermal point of view. A wider heating rate range as well as quantitative measurements of thermal events would be necessary to validate this observation.

4.2. Characterization of the microstructure

The SEM analyses were carried out for 5 characteristic temperatures (300 °C, 450 °C, 650 °C, 800 °C, 1200 °C). Sintering of the sample is observed before at 300 °C what can be associated with the start of sodium nitrate melting. As shown in Figure 3a and Figure 3b, no other microstructural change is observed. At 650 °C (Figure 3c) the glass frit have already softened, which is coherent with the value of the glass transition temperature of alumino-borosilicate glass frit (about 553 °C [26]). After the glass frit softening, the gases from the ongoing decomposition reactions remain trapped due to the mixture high viscosity at the temperature of 800 °C [28] and form bubbles which marks are shown in Figure 3d. Figure 3e illustrates the final state of the mixture at 1200 °C showing a quite complete homogeneity of the glass at the end of the heat treatment. This last observation validates the use of the run rerun method based on the assumption that all the reactions take place during the first run.

4.3. Identification of the main evolved gases

Figure 4a and Figure 4b show the normalized mass loss (TG), its time derivative (DTG), and intensity from mass spectroscopy. As shown in Figure 4a almost all of the mass loss takes place between 200 °C and 650 ° C and is associated to endothermic events. A peak with low intensity is detected around 1000 °C and can be associated with the volatility of some alkalis at high temperature. Five main gases CO_2, H_2O, OH, NO_2 and O_2 were identified by matching observed mass to charge ratio (m/z) patterns in MS with the spectroscopy database. A strong superposition of the gases characteristic curves can be observed. H_2O, OH are released from hydroxides, acids, and hydrates present in calcine [27]. NO_2 and O_2 gases can be associated with the decomposition reactions of nitrates still present in the calcine. CO_2 peak observed can be linked to the presence of carbon residue in the glass frit due to the manufacturing process using gas burning furnaces. The peaks of these gases intensity correspond at different points with the peaks of mass loss rate. With an appropriate calibration allowing to

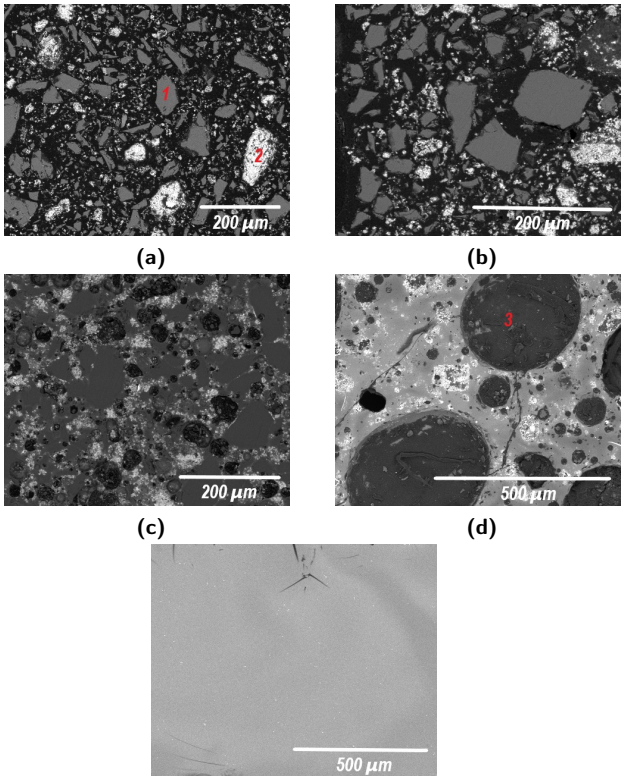

Figure 3: SEM images of the sample at different temperatures ((a) T=300 °C, (b) T=450 °C, (c) T=650 °C, (d) T= 800 °C, (e) T=1200 °C) during heating process at 10°C/min. 1 denotes a grain of glass frit, 2 denotes a grain of calcine and 3 the mark of the bubbles.

relate the intensity detected to the mass of gas, a modeling of the mass loss based on SM data can be used to describe a part of endothermic reactions [29–31]. The implementation of this method is not discussed in this paper.

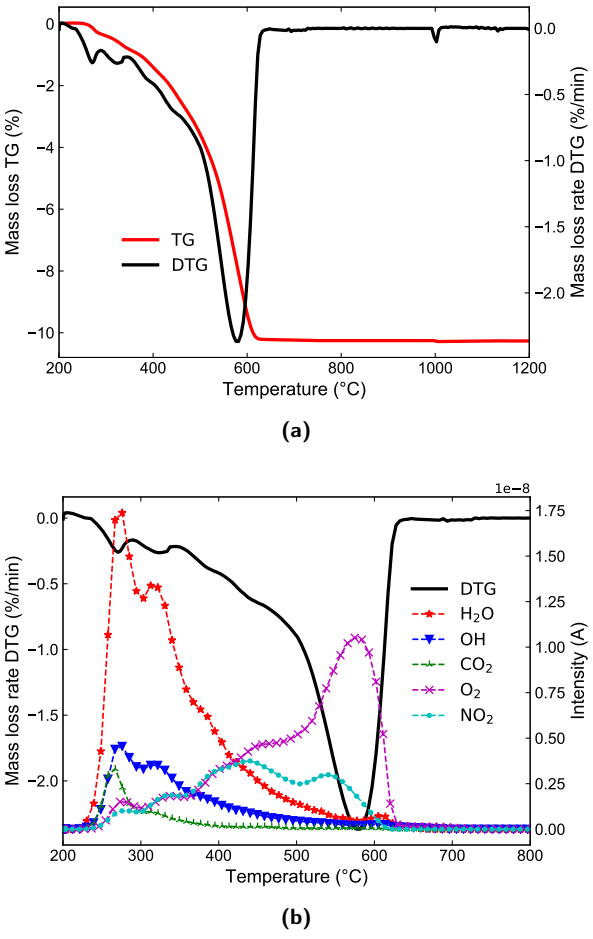

Figure 4: (a) Thermogravimetric data (TG and DTG) at 30 °C/min and (b) the intensity from mass spectroscopy.

4.4. Modeling results

For mathematical modeling, we focus on endothermic events which are predominant at high heating rate and which will have a thermal impact on the overall energy balance of the vitrification process. As shown in Figure 5 and based on F-Test analysis [32], four main peaks and shoulders are used to model the overall endothermic mechanism. Data processing and least squares methods have been solved using python 3.6.1 software.

Table 1
Apparent kinetic parameters values at different heating rate for each peak.

	$log A_i\ (s^{-1})$				n_i				w_i			
Peaks	1	2	3	4	1	2	3	4	1	2	3	4
5 °C/min	51.54	11.56	23.41	21.47	2.53	1.93	3.44	1.10	0.09	0.19	0.25	0.48
10 °C/min	52.11	12.09	23.70	21.51	3.87	4.58	2.39	1.45	0.10	0.30	0.17	0.43
20 °C/min	52.27	12.81	23.78	21.65	4.63	1.78	2.10	2.44	0.08	0.19	0.16	0.57
30 °C/min	52.23	13.30	23.52	21.53	4.10	2.96	3.98	1.99	0.08	0.25	0.25	0.42
40 °C/min	51.77	13.00	23.24	21.57	4.78	3.28	4.29	2.52	0.10	0.30	0.24	0.36
Average	51.98	12.55	23.53	21.55	3.98	2.90	3.24	1.90	0.09	0.24	0.22	0.45
RSD (%)	0.61	5.69	0.94	0.31	22.44	39.10	29.67	32.57	11.24	23.43	20.40	17.57

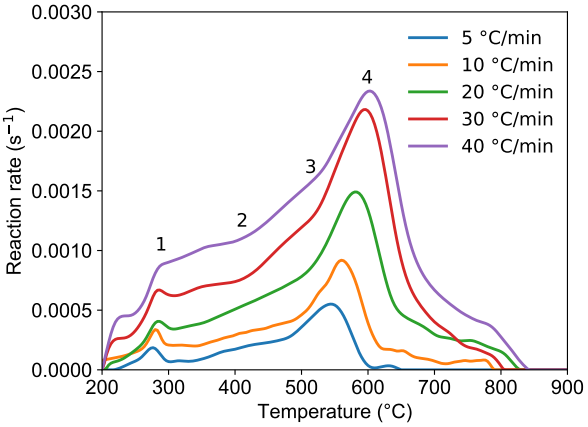

Figure 5: The reaction rate of endothermic part of mechanism for different heating rate.

To determine the apparent activation energy, Kissinger method is used. The slope of the plot of $(ln(\beta/T_{pi}^2)$ versus $(1/T_{pi})$ yields to $-E_i/R$. Figure 6 shows the Kissinger plots. We obtained the following values: 256.15 kJ/mol for peak 1 (R^2=0.965), 96.90 kJ/mol for peak 2 (R^2=0.947), 177.12 kJ/mol for peak 3 (R^2=0.991) and 186.24 kJ/mol for peak 4 (R^2=0.994). For each heating rate, the other apparent kinetics parameters (A_i, n_i, w_i) are identified using the least squares method.

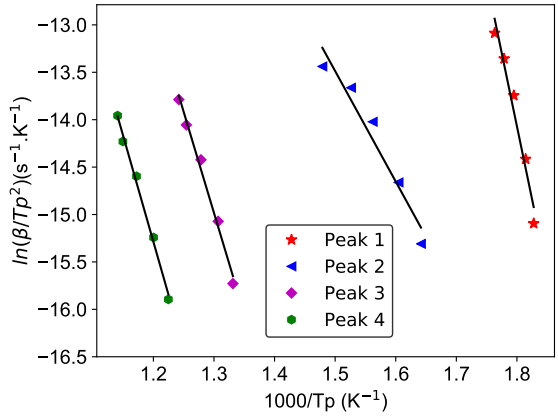

Figure 6: Kissinger plots used to determine the apparent activation energies of the four reactions identified. Black solid lines represent linear regression plots

The value of these parameters as well as the mean value and the relative standard deviation (RSD) for each peak are listed in Table 1. The pre-exponential factor values seem to be independant of the heating rate. A variability according to the heating rate is however observed for the reaction weight factor and for reaction order. Figure 7 shows the experimental, fitted and deconvolution curves for each heating rate.

By the fact that pre-exponential factor and the reaction order are intrinsic parameter of the reaction, they should be independent of heating rate. For this reason and with the aim of reducing the number of variable parameters, the average value of A_i and n_i are therefore used to recalculate the reaction weight factors through a second fit. The resulting curves are shown in Figure 8 and designated by «2^{nd} *fit*». The values of obtained w_i are listed in Table 2.

Table 2
Values of reaction weight factors (w_i) obtained after the second fit.

	Peaks			
β (°C/min)	1	2	3	4
5	0.08	0.14	0.25	0.54
10	0.09	0.23	0.19	0.48
20	0.08	0.27	0.18	0.47
30	0.09	0.28	0.18	0.45
40	0.10	0.34	0.17	0.39
Average	0.09	0.25	0.20	0.46
RSD (%)	13.09	29.97	16.57	11.59

The weight factor of reactions 1 and 3 respectively show a RSD of 13.09% and 16.57%. However, in the range of heating rates studied in this work, their variability does not show a clear trend. The reaction 2 with a RSD of 29.97% seems to increase with the rate of heating when the weight of peak 4 with a RSD of 11.59% decreases. This observed variability may be due to a modification from a phenomenological point of view of the reaction mechanism as a function of the imposed heat treatment. In such a case, the weight factor of the reactions would be a function of heating rate and consequently the hypothesis of independence of one reaction from another would be over-simplified. It should, however, be emphasized that this observed variability can be linked to the fact that the model did not perfectly match the experimental data as shown in

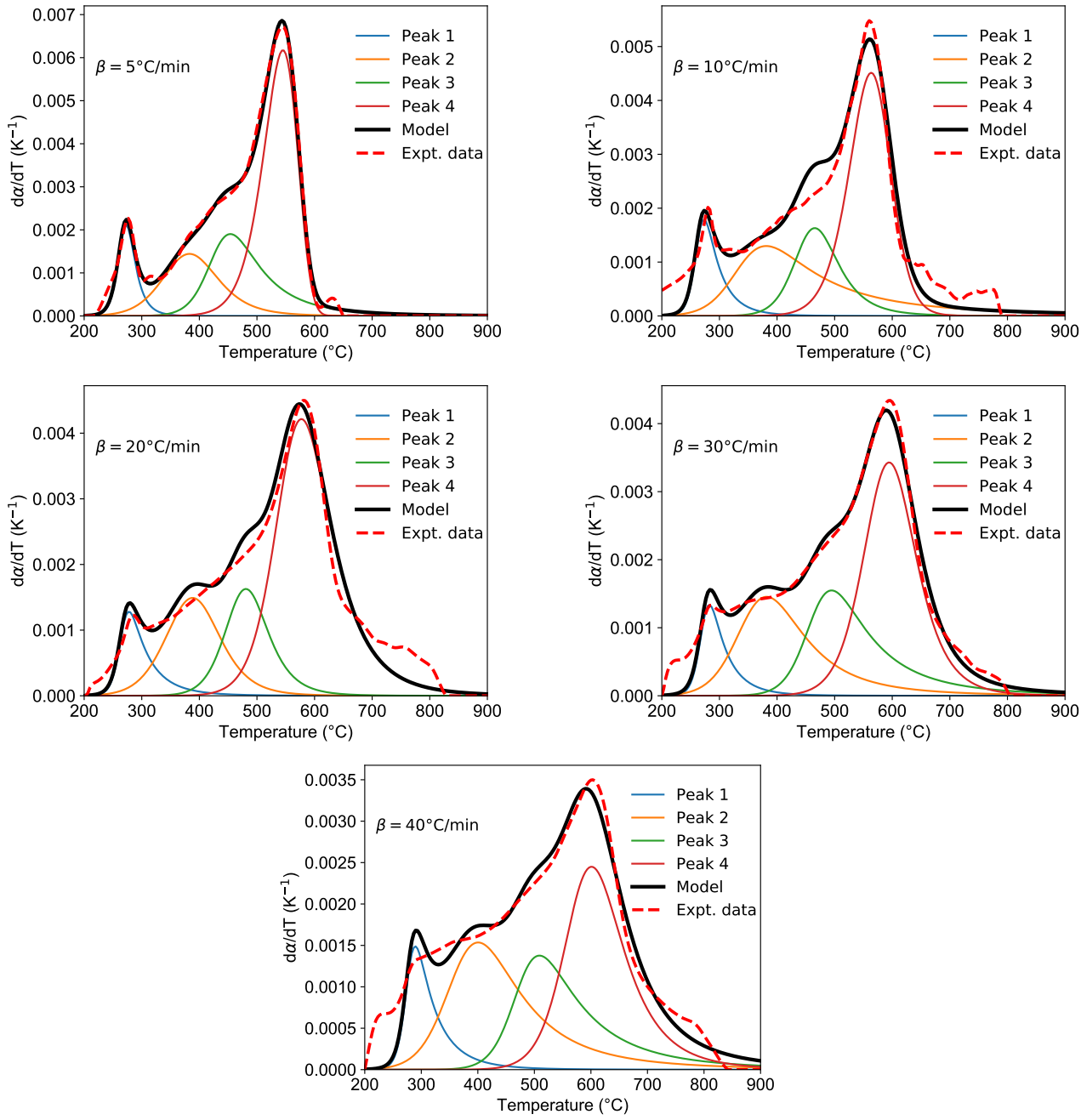

Figure 7: Experimental, fitted and deconvolution curves for heating rate of 5, 10, 20, 30, 40 °C/min.

Figure 8 and can also be the result of fluctuations generated by the experimental conditions where small mass of samples are used.

In the perspective of coupling this modeling of chemical kinetics with thermo-magneto-hydrodynamic simulations of the vitrification process in cold crucible, it would be preferable to have all kinetic parameters independent of the heating rate. This means that we will assume for CFD simulations that the chemical kinetics of endothermic reactions are independent of the heating rate. For this purpose, the mean values of the reaction weight factors listed in Table 2 associated with the mean values A_i and n_i listed in Table 1 are used to model the experimental data. The curves designated by «3^{rd} *fit*» in Figure 8 shows the result of the modeling. The fit is fairly approximate for the heating rate of 5 and 40 °C/min but nevertheless remains satisfactory for the heating rate of 10, 20, 30 °C/min.

5. Conclusion

Despite SEM and SM-TGA analyses providing information on the microstructural evolution and the nature of the evolved gases, it remains difficult to identify every single reaction occurring during the vitrification of

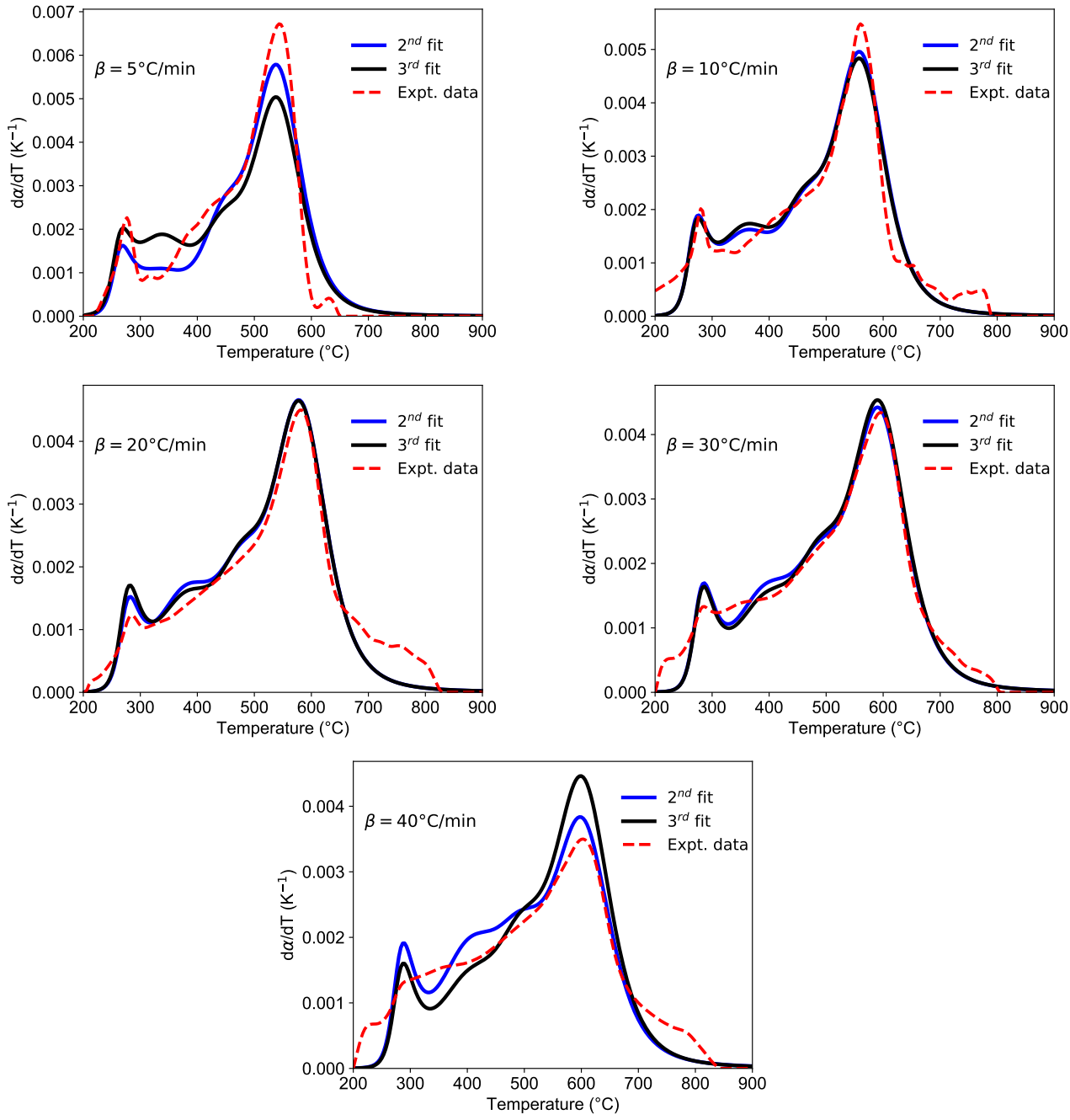

Figure 8: Experimental and fitted curves for heating rate of 5, 10, 20, 30, 40 °C/min. 2^{nd} fit denotes the modeling based on the use of the average values of A_i and n_i resulting from the 1^{st} fit. 3^{rd} fit designates the last modeling using the average values of w_i obtained from 2^{nd} fit coupled with the average values of A_i and n_i from the 1^{st} fit.

high level waste due to the complexity chemical system involved. This justifies the use of a global approach, such as DTA-TGA analyses used in this work, to describe the reaction mechanism. We have shown that the overall endothermic reactions mechanism, which are preponderant at high heating rate, can be satisfactorily described from a thermal point of view by a weighted sum of four n-order reactions. Such modeling can be used to track the evolution of chemical kinetics during the vitrification process. The quantification of reaction enthalpy associated with this mechanism through a simultaneous differential scanning calorimetry–thermogravimetry (DSC–TGA) would be necessary to take into account the thermal retroaction of chemistry on the overall energy balance inside the vitrification furnaces.

6. Aknowledgement

The authors are grateful to the Commissariat à l'Energie Atomique (CEA), to ORANO and EDF for their financial

support of this work. KEP Technologies is thanked for performing the TGA-MS measurements.

References

[1] R. Bonniaud, La vitrification en france des solutions de produits de fission, Nuclear Technology 34 (3) (1977) 449–460.

[2] E. Vernaz, J. Brueziere, History of nuclear waste glass in france, Procedia Materials Science 7 (2014) 3 – 9, 2nd International Summer School on Nuclear Glass Wasteform: Structure, Properties and Long-Term Behavior, SumGLASS 2013.

[3] R. Didierlaurent, A. Rodrigues, A. Ledoux, S. Schuller, C. Veyer, Nuclear liquid wastes calcination:the high-level french experience – 17184,wm2017 conference, 2017.

[4] H. Groot, K. Laevsky, A. Farina, A. Klar, R. Mattheij, A. Mikelić, N. Siedow, Mathematical Modelling of Glass Forming Processes, Vol. 2010, 2010, pp. 1–56.

[5] M. K. Choudhary, R. Venuturumilli, M. R. Hyre, Mathematical modeling of flow and heat transfer phenomena in glass melting, delivery, and forming processes, International Journal of Applied Glass Science 1 (2) (2010) 188–214.

[6] L. Li, H.-J. Lin, J. Han, J. Ruan, J. Xie, X. Zhao, Three-dimensional glass furnace model of combustion space and glass tank with electric boosting, MATERIALS TRANSACTIONS 60 (6) (2019) 1034–1043.

[7] A. Abbassi, K. Khoshmanesh, Numerical simulation and experimental analysis of an industrial glass melting furnace, Applied Thermal Engineering 28 (5) (2008) 450 – 459.

[8] D. Krause, H. Loch, Mathematical Simulation in Glass Technology, Springer-Verlag Berlin Heidelberg, 2002.

[9] R. Pokorny, P. Hrma, Mathematical modeling of cold cap, Journal of Nuclear Materials 429 (1) (2012) 245 – 256.

[10] R. Pokorný, P. Hrma, S. Lee, J. Klouzek, M. K. Choudhary, A. A. Kruger, Modeling batch melting: Roles of heat transfer and reaction kinetics, Journal of the American Ceramic Society 103 (2) (2020) 701–718.

[11] J. Chun, D. A. Pierce, R. Pokorny, P. Hrma, Cold-cap reactions in vitrification of nuclear waste glass: Experiments and modeling, Thermochimica Acta 559 (2013) 32 – 39.

[12] S. Primig, H. Leitner, Separation of overlapping retained austenite decomposition and cementite precipitation reactions during tempering of martensitic steel by means of thermal analysis, Thermochimica Acta 526 (1) (2011) 111 – 117.

[13] R. Pokorný, D. A. Pierce, P. Hrma, Melting of glass batch: Model for multiple overlapping gas-evolving reactions, Thermochimica Acta 541 (2012) 8 – 14.

[14] G. Suneel, S. Rajasekaran, J. Selvakumar, C. P. Kaushik, J. Gayen, K. Ravi, Determination of reaction kinetics during vitrification of radioactive liquid waste for different types of base glass, Nuclear Engineering and Technology 51 (3) (2019) 746 – 754.

[15] H. E. Kissinger, Reaction kinetics in differential thermal analysis, Analytical Chemistry 29 (11) (1957) 1702–1706.

[16] O. Pinet, S. Mure, Redox behavior of platinum-group metals in nuclear glass, Journal of Non-Crystalline Solids 355 (3) (2009) 221 – 227.

[17] B. Fleury, N. Godon, A. Ayral, D. Perret, J.-L. Dussossoy, S. Gin, Development of an experimental design to investigate the effects of r7t7 glass composition on the residual rate of alteration, Procedia Materials Science 7 (2014) 193 – 201, 2nd International Summer School on Nuclear Glass Wasteform: Structure, Properties and Long-Term Behavior, SumGLASS 2013.

[18] P. Frugier, C. Martin, I. Ribet, T. Advocat, S. Gin, The effect of composition on the leaching of three nuclear waste glasses: R7t7, avm and vrz, Journal of Nuclear Materials 346 (2) (2005) 194 – 207.

[19] S. Vyazovkin, A. K. Burnham, J. M. Criado, L. A. Pérez-Maqueda, C. Popescu, N. Sbirrazzuoli, Ictac kinetics committee recommendations for performing kinetic computations on thermal analysis data, Thermochimica Acta 520 (1) (2011) 1 – 19.

[20] M. E. Brown (Ed.), Reaction Kinetics from Thermal Analysis, Springer Netherlands, Dordrecht, 2001, pp. 181–214.

[21] A. K. Galwey, M. E. Brown, A theoretical justification for the application of the arrhenius equation to kinetics of solid state reactions (mainly ionic crystals), Proceedings of the Royal Society of London. Series A: Mathematical and Physical Sciences 450 (1995) 501 – 512.

[22] G. Senum, R. T. Yang, Rational approximations of the integral of the arrhenius function, Journal of thermal analysis 11 (1977) 445–447.

[23] P. Murray, J. White, Kinetics of the thermal dehydration of clays. iv. interpretationof the differential thermal analysis of the clay minerals, trans. brit. ceram.soc. 54 (1955) 204–237.

[24] Y. Han, Theoretical study of thermal analysis kinetics, Theses and Dissertations-Mechanical Engineering. 35.

[25] C. DOYLE, Series approximations to the equation of thermogravimetric data, Nature 207 (1965) 290–291.

[26] A. Monteiro, Etude des mecanismes de reactivite chimique des precurseurslors de l'elaboration d'un verre de confinement de dechet de haute activite :de l'experimentation a la modelisation, these de doctorat, de l'universite paulsabatier toulouse iii, Ph.D. thesis (2012).

[27] E. Boue, Etude de la reactivite chimique entre les precurseurs lors de l'elaboration de verres nucleaires enrichis en molybdene, Ph.D. thesis, thèse de doctorat dirigée par Toplis, Michael J. Sciences de la terre et des planètes solides Toulouse 3 2017 (2017).

[28] J. Puig, B. Penelon, P. Marchal, M. Neyret, Rheological properties of nuclear glass melt containing platinum group metals, Procedia Materials Science 7 (2014) 156 – 162, 2nd International Summer School on Nuclear Glass Wasteform: Structure, Properties and Long-Term Behavior, SumGLASS 2013.

[29] C. P. Rodriguez, J. Chun, M. J. Schweiger, A. A. Kruger, P. Hrma, Application of evolved gas analysis to cold-cap reactions of melter feeds for nuclear waste vitrification, Thermochimica Acta 592 (2014) 86 – 92.

[30] M. Maciejewski, A. Baiker, Quantitative calibration of mass spectrometric signals measured in coupled ta-ms system, Thermochimica Acta 295 (1) (1997) 95 – 105, coupling Thermal Analysis and Gas Analysis Methods.

[31] C.-A. Craig, K. E. Jarvis, L. J. Clarke, An assessment of calibration strategies for the quantitative and semi-quantitative analysis of calcium carbonate matrices by laser ablation-inductively coupled plasma-mass spectrometry (la-icp-ms), J. Anal. At. Spectrom. 15 (2000) 1001–1008.

[32] J. E. Freund, B. M. Perles, Modern elementary statistics 12th, 12th Edition, Prentice Hall,Upper Saddle River, NJ, 2006.